Journal of Quantitative Spectroscopy & Radiative Transfer 184 (2016) 180–192

Contents lists available at ScienceDirect

Journal of Quantitative Spectroscopy & Radiative Transfer

journal homepage: www.elsevier.com/locate/jqsrt

Multistatic aerosol–cloud lidar in space: A theoretical perspective

Michael I. Mishchenko [a,*], Mikhail D. Alexandrov [a,b], Brian Cairns [a], Larry D. Travis [a]

[a] NASA Goddard Institute for Space Studies, 2880 Broadway, New York, NY 10025, USA
[b] Department of Applied Physics and Applied Mathematics, Columbia University, 2880 Broadway, New York, NY 10025, USA

ARTICLE INFO

Article history:
Received 10 June 2016
Received in revised form
15 July 2016
Accepted 17 July 2016
Available online 21 July 2016

Keywords:
Aerosols
Clouds
Multistatic lidar
Electromagnetic scattering
Polarization

ABSTRACT

Accurate aerosol and cloud retrievals from space remain quite challenging and typically involve solving a severely ill-posed inverse scattering problem. In this Perspective, we formulate in general terms an aerosol and aerosol–cloud interaction space mission concept intended to provide detailed horizontal and vertical profiles of aerosol physical characteristics as well as identify mutually induced changes in the properties of aerosols and clouds. We argue that a natural and feasible way of addressing the ill-posedness of the inverse scattering problem while having an exquisite vertical-profiling capability is to fly a multistatic (including bistatic) lidar system. We analyze theoretically the capabilities of a formation-flying constellation of a primary satellite equipped with a conventional monostatic (backscattering) lidar and one or more additional platforms each hosting a receiver of the scattered laser light. If successfully implemented, this concept would combine the measurement capabilities of a passive multi-angle multi-spectral polarimeter with the vertical profiling capability of a lidar; address the ill-posedness of the inverse problem caused by the highly limited information content of monostatic lidar measurements; address the ill-posedness of the inverse problem caused by vertical integration and surface reflection in passive photopolarimetric measurements; help relax polarization accuracy requirements; eliminate the need for exquisite radiative-transfer modeling of the atmosphere–surface system in data analyses; yield the day-and-night observation capability; provide direct characterization of ground-level aerosols as atmospheric pollutants; and yield direct measurements of polarized bidirectional surface reflectance. We demonstrate, in particular, that supplementing the conventional backscattering lidar with just one additional receiver flown in formation at a scattering angle close to 170° can dramatically increase the information content of the measurements. Although the specific subject of this Perspective is the multistatic lidar concept, all our conclusions equally apply to a multistatic radar system intended to study from space the global distribution of cloud and precipitation characteristics.

Published by Elsevier Ltd.

1. Introduction

Tropospheric aerosols cause a significant radiative forcing of climate comparable, in the absolute-value sense, to that of the greenhouse gases [1–4]. However, the magnitude of this forcing remains highly uncertain because of inadequate quantitative knowledge of global aerosol characteristics and their temporal changes [4–10]. In fact, the persisting uncertainties in the aerosol direct and indirect radiative effects are so large that they preclude definitive climate model evaluation by comparison with observed global temperature change and must be reduced

* Corresponding author. Fax: +1 212 678 5622.
E-mail address: michael.i.mishchenko@nasa.gov (M.I. Mishchenko).

http://dx.doi.org/10.1016/j.jqsrt.2016.07.015
0022-4073/Published by Elsevier Ltd.

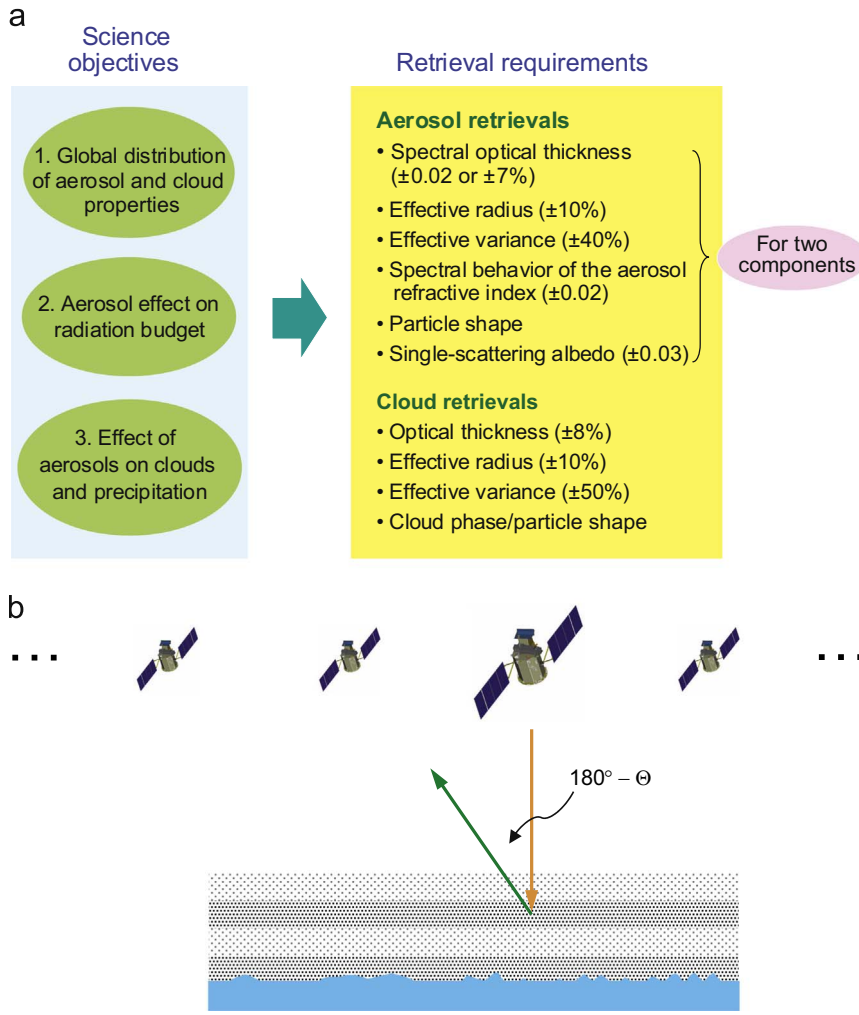

Fig. 1. (a) Aerosol and cloud retrieval requirements follow from the overarching science objectives. (b) Orbital multistatic lidar system. The primary satellite is equipped with a nadir-pointing backscattering lidar, while one or more secondary platforms carry additional receivers of scattered laser light. The scattering angle $\Theta \neq 180^\circ$ characterizes the bistatic configuration formed by the transmitted laser beam and the receiver on a secondary platform.

by at least a factor of three [11,12]. Achieving this goal requires a comprehensive global aerosol-monitoring program with three major science objectives shown in the left-hand panel of Fig. 1(a) [5]. The right-hand panel of Fig. 1(a) (after [13,14]) lists the minimal set of aerosol and cloud parameters that must be retrieved from space in order to enable a sufficiently accurate quantification of the aerosol effects on climate. The corresponding retrieval accuracy requirements are dictated by the need to detect changes of the aerosol direct and indirect radiative forcings estimated to be plausible during the next two decades and to determine quantitatively the contribution of these forcings to the planetary energy budget [13,15].

The characterization requirements summarized in Fig. 1(a) are quite challenging in terms of the number of retrieved parameters and the respective retrieval accuracies. As a consequence, the corresponding inverse remote-sensing problem can be severely ill-posed.

In the case of passive observations, each measurement typically integrates the scattering signal over the entire atmospheric column and convolves it with the polarized surface reflectance. The vertical resolution of passive photopolarimetric retrievals is thus inevitably rather crude. Furthermore, the analysis of passive data requires exquisite radiative-transfer modeling, while a stable solution of the inverse problem necessitates the use of a massively over-determined measurement dataset. The latter means that the individual units of data must be maximally independent in terms of their implicit information content, while their number must significantly exceed the number of unknown model parameters. This requires collecting as many units of data as possible by performing photopolarimetric observations of a scene from many different angles and at many wavelengths [14]. Moreover, multiple scattering of light weakens the resulting polarization [16,17], thereby necessitating an extremely high accuracy of polarimetric measurements (see, e.g., [18–21] and references therein).

Backscattering lidar observations employing a pulsed laser beam [22] are capable of providing much finer

vertical resolution than passive methodologies. However, even high spectral resolution lidar (HSRL) observations in three spectral channels typically yield only five units of data per elementary scattering volume from which one has to retrieve many more microphysical parameters of a potentially multi-component aerosol population (Fig. 1(a)). The ill-posedness of the resulting inverse problem has been well documented [23].

The main premise of this Perspective is that a natural and feasible way of addressing the ill-posedness of the aerosol and aerosol–cloud retrieval problem while having an exquisite vertical-profiling capability is to perform multistatic (including bistatic) lidar observations from space. We will show, in particular, that supplementing a conventional backscattering HSRL system with just one additional receiver flown in formation at a $\sim 170^\circ$ scattering angle more than triples the number of units of data while engaging elements of the scattering matrix much more sensitive to particle microphysical properties than the standard backscattering coefficient. Furthermore, this methodology helps decouple the surface and atmospheric contributions to the scattering signal and involves the measurement of single (rather than multiple) scattering of light by aerosol and cloud particles. As a consequence, cumbersome solutions of the vector radiative transfer equation are completely avoided, while the polarimetric accuracy requirements can be substantially relaxed.

2. Bistatic lidar equation

Over the past three decades, monostatic lidars (both elastic and HSRL) have contributed substantially to our knowledge of atmospheric composition. Owing to extensive research, the remote-sensing capabilities and limitations of these instruments are now well understood (see, e.g., [23–29] and references therein). In particular, there is compelling evidence that inversions of monostatic lidar observations cannot yield the entire set of the requisite aerosol characteristics and the requisite retrieval accuracies, as discussed in the preceding section. Therefore, in what follows we will focus on observation strategies involving multistatic lidars.

In the rest of this paper, we will use the following terminology. The term "bistatic lidar configuration" refers to the situation wherein the direction of the transmitted laser beam and the outward optical axis of the receiver are not co-aligned, i.e., the angle between the transmitted laser beam and the received scattered beam is not equal to 180°. The term "bistatic lidar system" refers to a combination of the conventional backscattering (i.e., monostatic) lidar and one additional receiver whose outward optical axis is not co-aligned with the direction of the transmitted laser beam. The term "multistatic lidar system" refers to a combination of the conventional monostatic lidar and $N \geq 1$ additional receivers whose outward optical axes point in different directions and are not co-aligned with the direction of the transmitted laser beam. Obviously, a multistatic lidar system with $N = 1$ is a bistatic system. The general geometric layout of a bistatic radar configuration and the corresponding equation were described in detail by Rogers and Eccles [30] and later adapted (in a simplified form) to lidar remote sensing by Reagan et al. [31,32].

In what follows, we will assume for simplicity that

- The Stokes parameters of both the transmitted and the scattered laser light are defined with respect to the scattering plane, i.e., the plane through the transmitted and scattered beams.
- The transmitted laser beam is pointed in the nadir direction (see Fig. 1(b)).
- All aerosol and cloud particles are either spherically symmetric or statistically isotropic and mirror-symmetric.

The first two assumptions imply that the scattering plane coincides with the meridional plane of the scattered beam. The third assumption implies that if the particles are not spherically symmetric then (i) they are randomly oriented and (ii) each of them has a plane of symmetry and/or is accompanied by a mirror counterpart [33-36].

Then the Stokes column vector of the scattered lidar return at the receiver,

$$\mathbf{I}^{\mathrm{sca}} = \begin{bmatrix} I^{\mathrm{sca}} \\ Q^{\mathrm{sca}} \\ U^{\mathrm{sca}} \\ V^{\mathrm{sca}} \end{bmatrix}, \tag{1}$$

can be expressed in terms of the Stokes column vector of the transmitted (incident) laser beam,

$$\mathbf{I}^{\mathrm{inc}} = \begin{bmatrix} I^{\mathrm{inc}} \\ Q^{\mathrm{inc}} \\ U^{\mathrm{inc}} \\ V^{\mathrm{inc}} \end{bmatrix}, \tag{2}$$

as follows:

$$\mathbf{I}^{\mathrm{sca}}(\Theta) = T_1 T_2(\Theta)\, \mathbf{F}^V(\Theta)\, \mathbf{I}^{\mathrm{inc}}, \tag{3}$$

where

- Θ is the scattering angle (i.e., the angle between the incidence and scattering directions, Fig. 1(b)).
- T_1 is the scalar exponential attenuation factor corresponding to the vertical light path from the laser to the scattering volume.
- $T_2(\Theta)$ is the scalar exponential attenuation factor corresponding to the slanted light path from the scattering volume to the receiver (for a monostatic backscattering lidar, $\Theta = 180^\circ$ and $T_2(180^\circ) \equiv T_1$).
- $\mathbf{F}^V(\Theta)$ is the local scattering matrix per unit volume of the atmosphere.

The Stokes parameters are defined according to [34,36] assuming the $\exp(-\mathrm{i}\omega t)$ time-harmonic dependence of the electromagnetic field, where $\mathrm{i} = (-1)^{1/2}$, ω is the angular frequency, and t is time. Implicit arguments in all quantities entering Eq. (3) are the wavelength of observations λ and (with the exception of $\mathbf{I}^{\mathrm{inc}}$) the coordinates of the scattering volume.

Note that strictly speaking, the actual polarized reading of the receiver is equal to the product of the right-hand side of Eq. (3) and a factor that depends on the specific geometry of the transmitter–receiver configuration in Fig. 1(b) while being independent of any of the atmospheric optical parameters [30,31]. We will assume that this geometric factor is always known and can be omitted for simplicity, thereby yielding Eq. (3).

In general, the *volume* scattering matrix has a particulate and a Rayleigh component:

$$\mathbf{F}^V(\Theta)=\frac{k^{\mathrm{p}}_{\mathrm{sca}}}{4\pi}\,\mathbf{F}^{\mathrm{p}}(\Theta)+\frac{k^{\mathrm{R}}_{\mathrm{sca}}}{4\pi}\,\mathbf{F}^{\mathrm{R}}(\Theta), \tag{4}$$

where

- $\mathbf{F}^{\mathrm{p}}(\Theta)$ is the 4×4 *normalized* particulate (aerosol and/or cloud) scattering matrix [34,36].
- $\mathbf{F}^{\mathrm{R}}(\Theta)$ is the *normalized* Rayleigh scattering matrix.
- $k^{\mathrm{p}}_{\mathrm{sca}}$ and $k^{\mathrm{R}}_{\mathrm{sca}}$ are the particulate and Rayleigh volume scattering coefficients, respectively.

The (1, 1) elements of the particulate and Rayleigh scattering matrices (i.e., the corresponding phase functions) are normalized according to

$$\frac{1}{2}\int_0^{\pi}\mathrm{d}\Theta\,F^{\mathrm{p}}_{11}(\Theta)\sin\Theta=\frac{1}{2}\int_0^{\pi}\mathrm{d}\Theta\,F^{\mathrm{R}}_{11}(\Theta)\sin\Theta=1. \tag{5}$$

The vertical profile of the Rayleigh scattering coefficient $k^{\mathrm{R}}_{\mathrm{sca}}$ is usually assumed to be known.

The Rayleigh scattering matrix is given by [16,33]

$$\mathbf{F}^{\mathrm{R}}(\Theta)=\frac{3}{4}\begin{bmatrix}1+\cos^2\Theta & -\sin^2\Theta & 0 & 0\\ -\sin^2\Theta & 1+\cos^2\Theta & 0 & 0\\ 0 & 0 & 2\cos\Theta & 0\\ 0 & 0 & 0 & 2\cos\Theta\end{bmatrix}, \tag{6}$$

while the particulate scattering matrix has the following block-diagonal structure [33–36]:

$$\mathbf{F}^{\mathrm{p}}(\Theta)=\begin{pmatrix}F^{\mathrm{p}}_{11}(\Theta) & F^{\mathrm{p}}_{12}(\Theta) & 0 & 0\\ F^{\mathrm{p}}_{12}(\Theta) & F^{\mathrm{p}}_{22}(\Theta) & 0 & 0\\ 0 & 0 & F^{\mathrm{p}}_{33}(\Theta) & F^{\mathrm{p}}_{34}(\Theta)\\ 0 & 0 & -F^{\mathrm{p}}_{34}(\Theta) & F^{\mathrm{p}}_{44}(\Theta)\end{pmatrix}, \tag{7}$$

with only six independent elements and with

$$F^{\mathrm{p}}_{12}(180^\circ)=0,\quad F^{\mathrm{p}}_{34}(180^\circ)=0, \tag{8}$$

$$F^{\mathrm{p}}_{33}(180^\circ)=-F^{\mathrm{p}}_{22}(180^\circ). \tag{9}$$

In addition [34],

$$F^{\mathrm{p}}_{44}(180^\circ)=F^{\mathrm{p}}_{11}(180^\circ)-2F^{\mathrm{p}}_{22}(180^\circ),\quad F^{\mathrm{p}}_{22}(180^\circ)\geq 0. \tag{10}$$

Furthermore, in the case of spherically symmetric particles

$$F^{\mathrm{p}}_{22}(\Theta)\equiv F^{\mathrm{p}}_{11}(\Theta), \tag{11}$$

$$F^{\mathrm{p}}_{44}(\Theta)\equiv F^{\mathrm{p}}_{33}(\Theta), \tag{12}$$

$$F^{\mathrm{p}}_{33}(180^\circ)=F^{\mathrm{p}}_{44}(180^\circ)=-F^{\mathrm{p}}_{11}(180^\circ). \tag{13}$$

It is easily seen that the volume scattering matrix also has the structure defined by Eqs. (7)–(13). Specifically,

$$\mathbf{F}^V(\Theta)=\begin{pmatrix}F^V_{11}(\Theta) & F^V_{12}(\Theta) & 0 & 0\\ F^V_{12}(\Theta) & F^V_{22}(\Theta) & 0 & 0\\ 0 & 0 & F^V_{33}(\Theta) & F^V_{34}(\Theta)\\ 0 & 0 & -F^V_{34}(\Theta) & F^V_{44}(\Theta)\end{pmatrix}, \tag{14}$$

$$F^V_{12}(180^\circ)=0,\quad F^V_{34}(180^\circ)=0, \tag{15}$$

$$F^V_{33}(180^\circ)=-F^V_{22}(180^\circ), \tag{16}$$

$$F^V_{44}(180^\circ)=F^V_{11}(180^\circ)-2F^V_{22}(180^\circ),\quad F^V_{22}(180^\circ)\geq 0, \tag{17}$$

and, in the case of spherically symmetric particles,

$$F^V_{22}(\Theta)\equiv F^V_{11}(\Theta), \tag{18}$$

$$F^V_{44}(\Theta)\equiv F^V_{33}(\Theta), \tag{19}$$

$$F^V_{33}(180^\circ)=F^V_{44}(180^\circ)=-F^V_{11}(180^\circ). \tag{20}$$

3. Multistatic system of lidar equations

Let us now assume that the multistatic lidar system in Fig. 1(b) includes $N\geq 0$ secondary receivers and thereby yields $N+1$ simultaneous photopolarimetric measurements for each scattering volume. We therefore have the following multistatic system of lidar equations that establishes the relation of the lidar observables to the aerosol and/or cloud characteristics of the scattering volume:

$$\begin{cases}\mathbf{I}^{\mathrm{sca}}(180^\circ)=T_1^2\,\mathbf{F}^V(180^\circ)\mathbf{I}^{\mathrm{inc}}\\ \mathbf{I}^{\mathrm{sca}}(\Theta_1)=T_1T_2(\Theta_1)\,\mathbf{F}^V(\Theta_1)\mathbf{I}^{\mathrm{inc}}\\ \ldots\\ \mathbf{I}^{\mathrm{sca}}(\Theta_N)=T_1T_2(\Theta_N)\,\mathbf{F}^V(\Theta_N)\mathbf{I}^{\mathrm{inc}}.\end{cases} \tag{21}$$

The first equation of this system is the full polarization version of the standard backscattering-lidar equation [24,25,27].

The systems (21) written for different individual scattering volumes are not mutually independent and are coupled through the exponential attenuation factors T_1 and $T_2(\Theta)$. Indeed, these factors include an integral of the particulate+gaseous extinction coefficient $k^V_{\mathrm{ext}}=k^{\mathrm{p}}_{\mathrm{ext}}+k^{\mathrm{R}}_{\mathrm{ext}}$ over a vertical (T_1) or a slanted (T_2) path. In other words, the systems (21) can be thought of as forming a "super-system" of equations coupled through the factors T_1 and $T_2(\Theta)$ either vertically (if $N=0$) or both vertically and horizontally (if $N\geq 1$). The horizontal coupling occurs through the factor $T_2(\Theta)$ and vanishes only if the atmosphere can be considered horizontally homogeneous so that

$$T_2(\Theta)=\exp(\ln T_1/\cos\Theta). \tag{22}$$

Importantly, HSRL measurements can yield the attenuation factors T_1^2 and $T_1T_2(\Theta)$ directly. This helps fully decouple the systems (21) pertaining to different

scattering volumes and thereby dramatically simplify the formulation and solution of the inverse scattering problem.

In general, the practical solution of a polystatic super-system of lidar equations can be highly involved, especially in the case of an elastic (non-HSRL) lidar (cf. the discussion of monostatic lidar retrievals in [24,25,27]), and will not be addressed specifically. Instead, we will analyze how different observation strategies can be used to maximize the implicit information content of the lidar measurements and thereby ameliorate the ill-posedness of the inverse remote-sensing problem.

4. Polarization scenarios

In what follows, the transmitted laser beam will be assumed to be fully polarized such that besides the intensity $I^{\rm inc}$, only one other Stokes parameter ($Q^{\rm inc}$, $U^{\rm inc}$, or $V^{\rm inc}$) is nonzero and is equal to $\pm I^{\rm inc}$. It is then straightforward to see that it is sufficient to consider only the following three combinations of the transmitted and the resulting scattered Stokes vector, where the subscripts Q, U, and V serve to discriminate between the three incident-polarization scenarios:

$$\mathbf{I}_Q^{\rm inc}=\begin{bmatrix} I^{\rm inc}\\ I^{\rm inc}\\ 0\\ 0\end{bmatrix},\quad \mathbf{I}_Q^{\rm sca}(\Theta)=T_1T_2(\Theta)\begin{bmatrix} [F_{11}^V(\Theta)+F_{12}^V(\Theta)]I^{\rm inc}\\ [F_{12}^V(\Theta)+F_{22}^V(\Theta)]I^{\rm inc}\\ 0\\ 0\end{bmatrix}, \tag{23}$$

$$\mathbf{I}_U^{\rm inc}=\begin{bmatrix} I^{\rm inc}\\ 0\\ I^{\rm inc}\\ 0\end{bmatrix},\quad \mathbf{I}_U^{\rm sca}(\Theta)=T_1T_2(\Theta)\begin{bmatrix} F_{11}^V(\Theta)I^{\rm inc}\\ F_{12}^V(\Theta)I^{\rm inc}\\ F_{33}^V(\Theta)I^{\rm inc}\\ -F_{34}^V(\Theta)I^{\rm inc}\end{bmatrix}, \tag{24}$$

$$\mathbf{I}_V^{\rm inc}=\begin{bmatrix} I^{\rm inc}\\ 0\\ 0\\ I^{\rm inc}\end{bmatrix},\quad \mathbf{I}_V^{\rm sca}(\Theta)=T_1T_2(\Theta)\begin{bmatrix} F_{11}^V(\Theta)I^{\rm inc}\\ F_{12}^V(\Theta)I^{\rm inc}\\ F_{34}^V(\Theta)I^{\rm inc}\\ F_{44}^V(\Theta)I^{\rm inc}\end{bmatrix}. \tag{25}$$

Eqs. (23) and (24) describe two alternative cases of a linearly polarized transmitted laser beam, while Eq. (25) describes the case of circularly polarized laser light.

5. Elastic lidar

Let us first consider the case of a non-HSRL lidar. It follows immediately from Eqs. (15)–(20) that in the case of spherically symmetric particles and a conventional monostatic lidar ($N=0$, $\Theta=180^\circ$), the only measureable quantity carrying useful information is the twice-attenuated backscattering coefficient $T_1^2F_{11}^V(180^\circ)$. Indeed, then

$$\mathbf{I}_Q^{\rm sca}(180^\circ)=T_1^2\begin{bmatrix} F_{11}^V(180^\circ)I^{\rm inc}\\ F_{11}^V(180^\circ)I^{\rm inc}\\ 0\\ 0\end{bmatrix}, \tag{26}$$

$$\mathbf{I}_U^{\rm sca}(180^\circ)=T_1^2\begin{bmatrix} F_{11}^V(180^\circ)I^{\rm inc}\\ 0\\ -F_{11}^V(180^\circ)I^{\rm inc}\\ 0\end{bmatrix}, \tag{27}$$

$$\mathbf{I}_V^{\rm sca}(180^\circ)=T_1^2\begin{bmatrix} F_{11}^V(180^\circ)I^{\rm inc}\\ 0\\ 0\\ -F_{11}^V(180^\circ)I^{\rm inc}\end{bmatrix}. \tag{28}$$

Measuring $T_1^2F_{11}^V(180^\circ)$ at (typically) three laser wavelengths triples the number of units of data and thereby increases the amount of implicit information. Still this information is quite limited and insufficient for a reliable solution of the inverse scattering problem involving many more unknown parameters, as discussed in Section 1.

It follows from Eqs. (23)–(25) that using just one extra receiver at $\Theta_1\neq 180^\circ$ brings into play as many as three additional nonzero scattering matrix elements. The actual use of the quantities $T_1T_2(\Theta)[F_{11}^V(\Theta)+F_{12}^V(\Theta)]$ (Eq. (23)) and $T_1T_2(\Theta)F_{11}^V(\Theta)$ (Eqs. (24) and (25)) can be problematic if the atmosphere is strongly inhomogeneous in the horizontal direction, in which case Eq. (22) is invalid and the systems (21) remain coupled horizontally. However, the normalization of the second, third, and fourth elements of the scattered Stokes column vectors in Eqs. (23)–(25) by the first element yields fully decoupled (both vertically and horizontally) ratios $[F_{12}^V(\Theta)+F_{22}^V(\Theta)]/[F_{11}^V(\Theta)+F_{12}^V(\Theta)]$, $F_{33}^V(\Theta)/F_{11}^V(\Theta)$, $F_{12}^V(\Theta)/F_{11}^V(\Theta)$, and $F_{34}^V(\Theta)/F_{11}^V(\Theta)$ (we still assume spherically symmetric particles). This results in a complete horizontal decoupling of the systems (21), which can be expected to substantially simplify the solution of the inverse problem. It is also obvious that the U and V polarization scenarios (Eqs. (24) and (25)) are much more beneficial than the Q scenario (Eq. (23)) in that adding just one receiver at $\Theta_1\neq 180^\circ$ serves to quadruple the number of units of measurement data. Furthermore, we will demonstrate in the following section that the ratios $F_{33}^V(\Theta)/F_{11}^V(\Theta)$, $F_{12}^V(\Theta)/F_{11}^V(\Theta)$, and $F_{34}^V(\Theta)/F_{11}^V(\Theta)$ can be expected to be even more sensitive to the particle microphysics than the standard attenuated backscattering coefficient. Using $N\geq 2$ additional receivers increases the information content even further.

The full numerical solution of the super-system of polystatic lidar equations could be iterative in nature and proceed along the following broad outline (suggested by the anonymous reviewer):

1. Assume for some Δz (linked to the turbidity of the aerosol layer, where z is the vertical coordinate) the microphysical model of the underlying aerosol, which allows for the estimate of the lidar extinction-to-backscatter ratio (or other intensive properties needed for polarized lidar).

2. Integrate the nadir-backscatter lidar equation over z, thereby obtaining the transmission factors needed to correct the lidar scattering returns for nadir geometry.
3. Using the measured polarization ratios within the proposed system architecture, obtain improved microphysical parameters of the aerosol model.
4. Using the improved microphysical model, return to step 1 and recalculate the lidar extinction-to-backscatter ratio, and then proceed iteratively to some convergence.

6. HSRL

The HSRL technique [37–39] uses spectral broadening of the lidar return from the gaseous atmosphere, which allows for the separation between the gaseous and particulate returns. As a consequence, an HSRL measurement can yield directly the product $T_1T_2(\Theta)$ and, thus, the product $k^{\rm p}_{\rm sca}\mathbf{F}^{\rm p}(\Theta)$. In particular, the measurements of the particulate extinction coefficient $k^{\rm p}_{\rm ext}$ and the particulate volume scattering matrix $k^{\rm p}_{\rm sca}\mathbf{F}^{\rm p}(\Theta)$ for all individual scattering volumes (and thus the corresponding inverse problems) become fully decoupled. As a consequence, each elementary scattering volume can be characterized by the following set of optical observables:

$$\begin{cases} k^{\rm p}_{\rm ext} \\ k^{\rm p}_{\rm sca}\mathbf{F}^{\rm p}(180^\circ) \\ k^{\rm p}_{\rm sca}\mathbf{F}^{\rm p}(\Theta_1) \\ k^{\rm p}_{\rm sca}\mathbf{F}^{\rm p}(\Theta_2) \\ \ldots \\ k^{\rm p}_{\rm sca}\mathbf{F}^{\rm p}(\Theta_N). \end{cases} \tag{29}$$

Besides $k^{\rm p}_{\rm ext}$, the only measureable quantity carrying supplementary information in the case of a monostatic HSRL and spherical particles is the particulate backscattering coefficient $k^{\rm p}_{\rm sca}F^{\rm p}_{11}(180^\circ)$. An example of using the values of $k^{\rm p}_{\rm ext}$ and $k^{\rm p}_{\rm sca}F^{\rm p}_{11}(180^\circ)$ measured at two HSRL wavelengths (typically 355 and 532 nm) and the value of the twice-attenuated backscattering coefficient $T_1^2F^V_{11}(180^\circ)$ at a third elastic wavelength (typically 1064 nm) is the so-called "$3\beta+2\alpha$" technique [29,40–44]. With only five units of data per scattering volume, this technique has been demonstrated to be incapable of solving the ill-posed inverse particle-characterization problem involving many more unknown parameters than five [23].

Placing another receiver at $\Theta_1 \neq 180^\circ$ and using either the U or the V polarization scenario serves to engage as many as four additional units of data in each HSRL spectral channel per individual scattering volume containing spherically symmetric particles: $k^{\rm p}_{\rm sca}F^{\rm p}_{11}(\Theta)$, $k^{\rm p}_{\rm sca}F^{\rm p}_{33}(\Theta)$, $k^{\rm p}_{\rm sca}F^{\rm p}_{12}(\Theta)$, and $k^{\rm p}_{\rm sca}F^{\rm p}_{34}(\Theta)$. Furthermore, the measurements in the additional elastic channel engage the fully decoupled ratios $F^V_{33}(\Theta)/F^V_{11}(\Theta)$, $F^V_{12}(\Theta)/F^V_{11}(\Theta)$, and $F^V_{34}(\Theta)/F^V_{11}(\Theta)$. The resulting number of units of data measured in the three spectral channels now exceeds the number of unknown model parameters discussed in Section 1, thereby likely making the inverse scattering problem sufficiently well posed. Needless to say, adding more receivers can be expected to make the solution of the inverse problem even more stable.

The key advantage of the quantities $F^{\rm p}_{11}(\Theta)$, $F^{\rm p}_{33}(\Theta)$, $F^{\rm p}_{12}(\Theta)$, and $F^{\rm p}_{34}(\Theta)$ is that they can be extremely sensitive to particle microphysics at certain scattering angles. To demonstrate that, Figs. 2–5 show the results of Lorenz–Mie computations for a gamma size distribution [16,34] of nonabsorbing spherical aerosols with refractive indices m varying between 1.35 and 1.6. Each ratio is plotted versus the scattering angle $\Theta \in [90^\circ, 180^\circ]$ and effective size parameter $x_{\rm eff} = 2\pi r_{\rm eff}/\lambda$, where $r_{\rm eff}$ is the effective radius [16,34]. The effective variance of the size distribution is fixed at a value $v_{\rm eff} = 0.2$ characteristic of a moderately broad polydispersion of radii. It is obvious that the sensitivity of all four ratios depicted in Figs. 2–5 to particle microphysics is indeed quite strong at side-scattering and near-backscattering angles. Note that unlike the ratio $F^{\rm p}_{11}(\Theta)/F^{\rm p}_{11}(180^\circ)$, the ratios $F^{\rm p}_{33}(\Theta)/F^{\rm p}_{11}(\Theta)$, $-F^{\rm p}_{12}(\Theta)/F^{\rm p}_{11}(\Theta)$, and $F^{\rm p}_{34}(\Theta)/F^{\rm p}_{11}(\Theta)$ can change not only their magnitude but also their sign, which makes them even more sensitive to m and $r_{\rm eff}$.

Fig. 6 further illustrates this sensitivity by providing the vertical cross sections of the two-dimensional panels in Figs. 2–5 corresponding to the scattering angle $\Theta = 170^\circ$. This angle appears to be near-optimal in the case of an orbital lidar system involving only one additional receiver. The ranges of variability of all four ratios in Fig. 6 are quite wide and become even more impressive upon recalling that in the case of a monostatic laser system, $-F^{\rm p}_{12}(180^\circ)/F^{\rm p}_{11}(180^\circ) = F^{\rm p}_{34}(180^\circ)/F^{\rm p}_{11}(180^\circ) \equiv 0$ and $F^{\rm p}_{33}(180^\circ)/F^{\rm p}_{11}(180^\circ) \equiv -100\%$.

7. Discussion and concluding remarks

The overall objective of this Perspective is to formulate in very general terms an aerosol and aerosol–cloud interaction space mission concept intended to determine:

- The horizontal and vertical profiles of aerosol micro- and macrophysical properties and how they change in the vicinity of clouds; and
- Changes in cloud properties in the presence of aerosols.

Specifically, we have analyzed theoretically a multistatic lidar mission as a formation-flying constellation of a primary satellite equipped with a monostatic backscattering lidar (elastic or HSRL) and one or more additional platforms each hosting a receiver of the scattered laser light. If successfully implemented, this concept would:

- Combine the measurement capabilities of a passive multi-angle multi-spectral polarimeter with the vertical profiling capability of a lidar.
- Ameliorate the ill-posed nature of the inverse scattering problem caused by vertical integration and surface reflection in passive photopolarimetric measurements.
- Ameliorate the ill-posed nature of the inverse scattering problem inherent in monostatic lidar retrievals and caused by a highly limited amount of information implicit in the measurements.
- Help relax polarization accuracy requirements.
- Eliminate the need for exquisite radiative-transfer modeling of the atmosphere–surface system in data analyses.
- Yield the day-and-night observation capability.

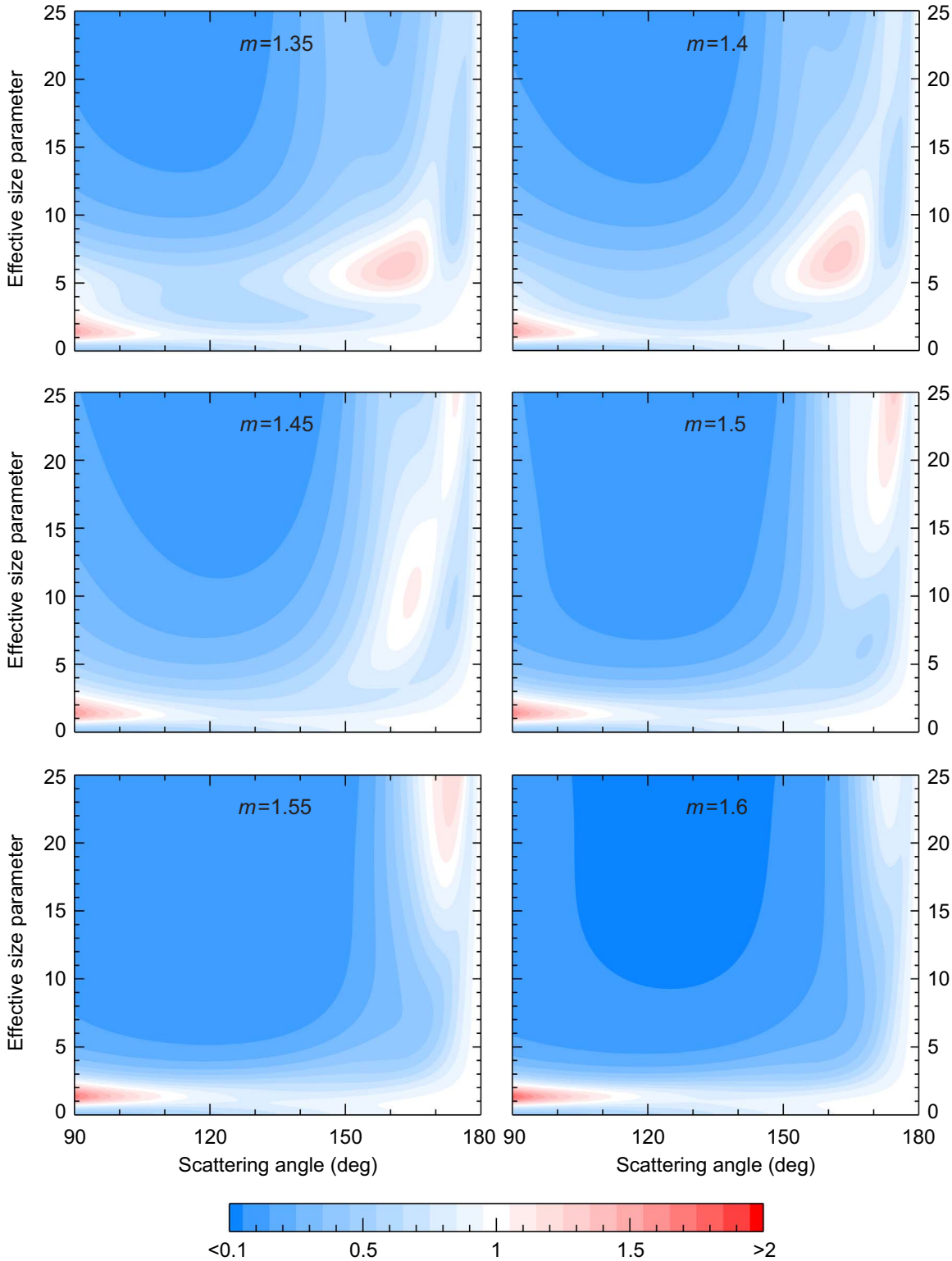

Fig. 2. Color contour plots of the ratio $F_{11}^{p}(\Theta)/F_{11}^{p}(180^{\circ})$ vs. effective size parameter and scattering angle for polydisperse spherical particles. The particle refractive index m is real-valued and ranges from 1.35 to 1.6.

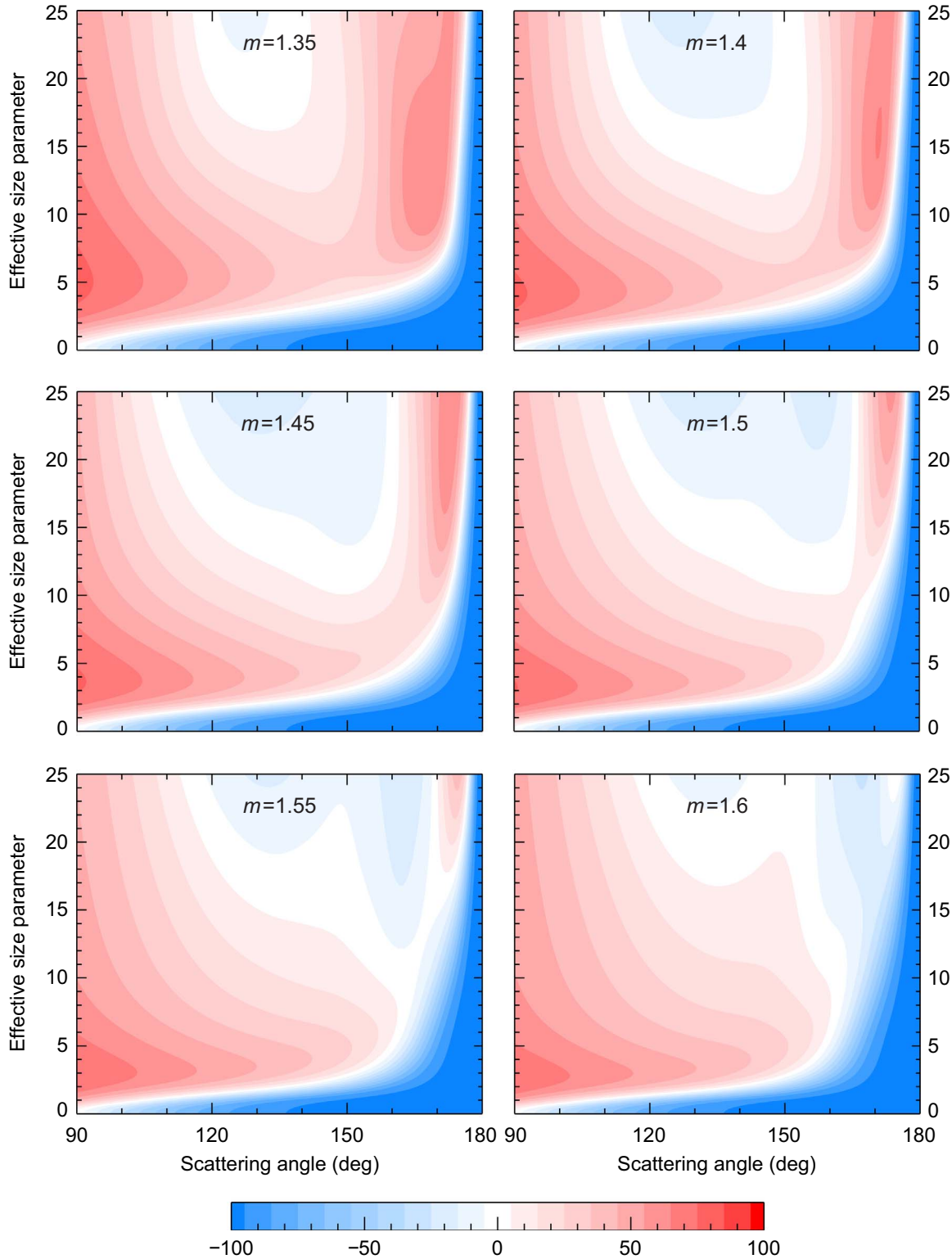

Fig. 3. As in Fig. 2, but for the ratio $F^{p}_{33}(\Theta)/F^{p}_{11}(\Theta)$ (in %).

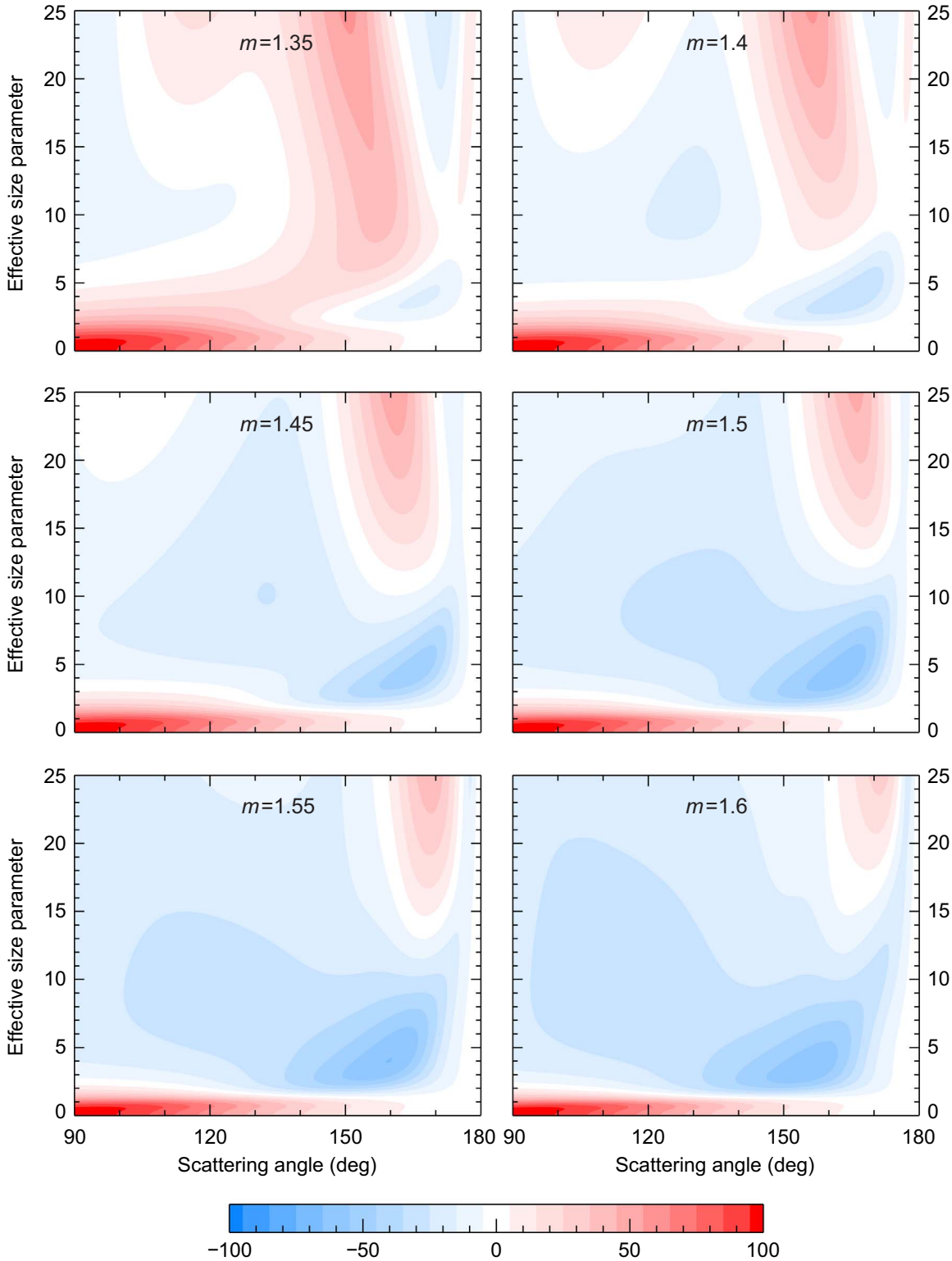

Fig. 4. As in Fig. 2, but for the ratio $-F_{12}^{\mathrm{p}}(\Theta)/F_{11}^{\mathrm{p}}(\Theta)$ (in %).

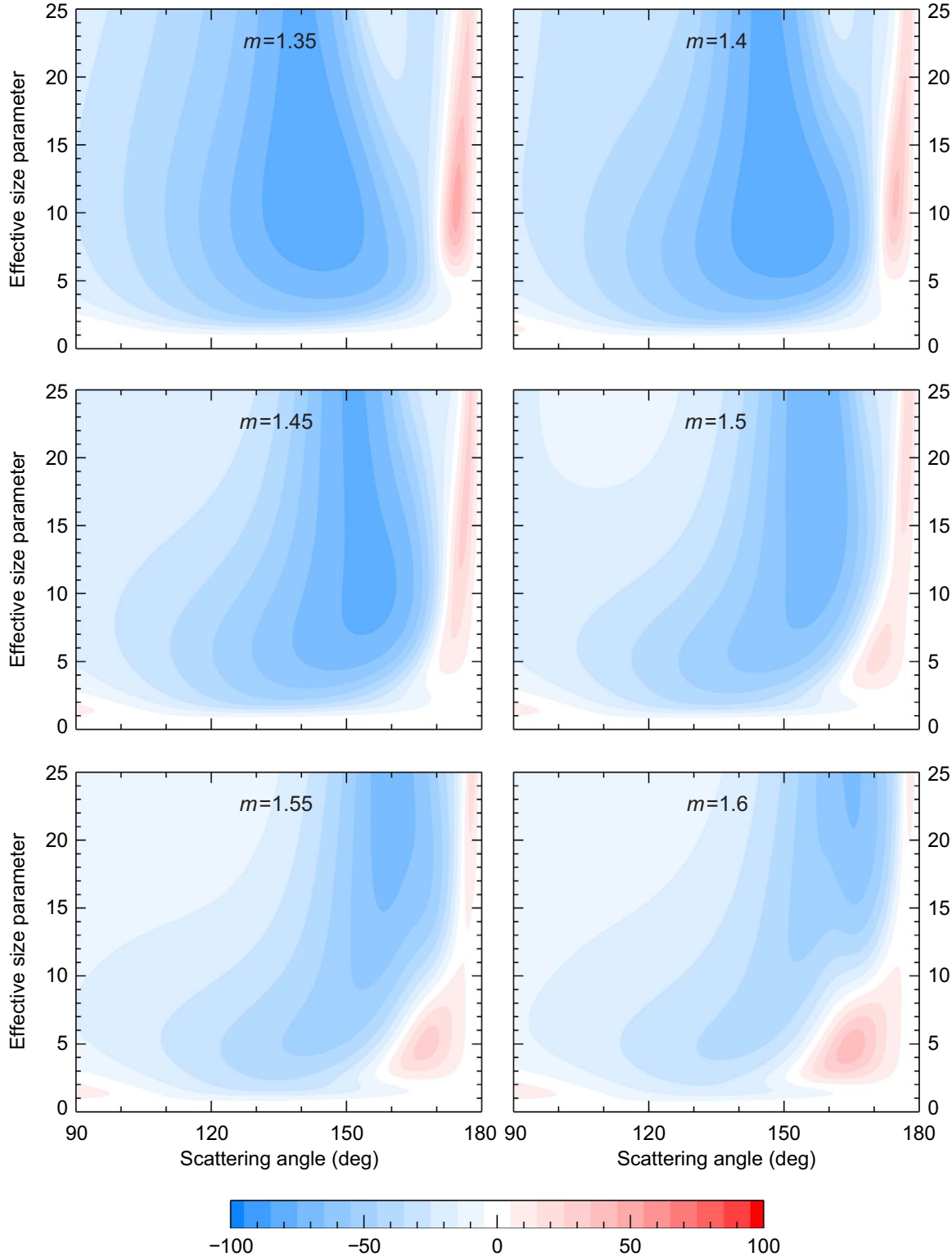

Fig. 5. As in Fig. 2, but for the ratio $F_{34}^{p}(\Theta)/F_{11}^{p}(\Theta)$ (in %).

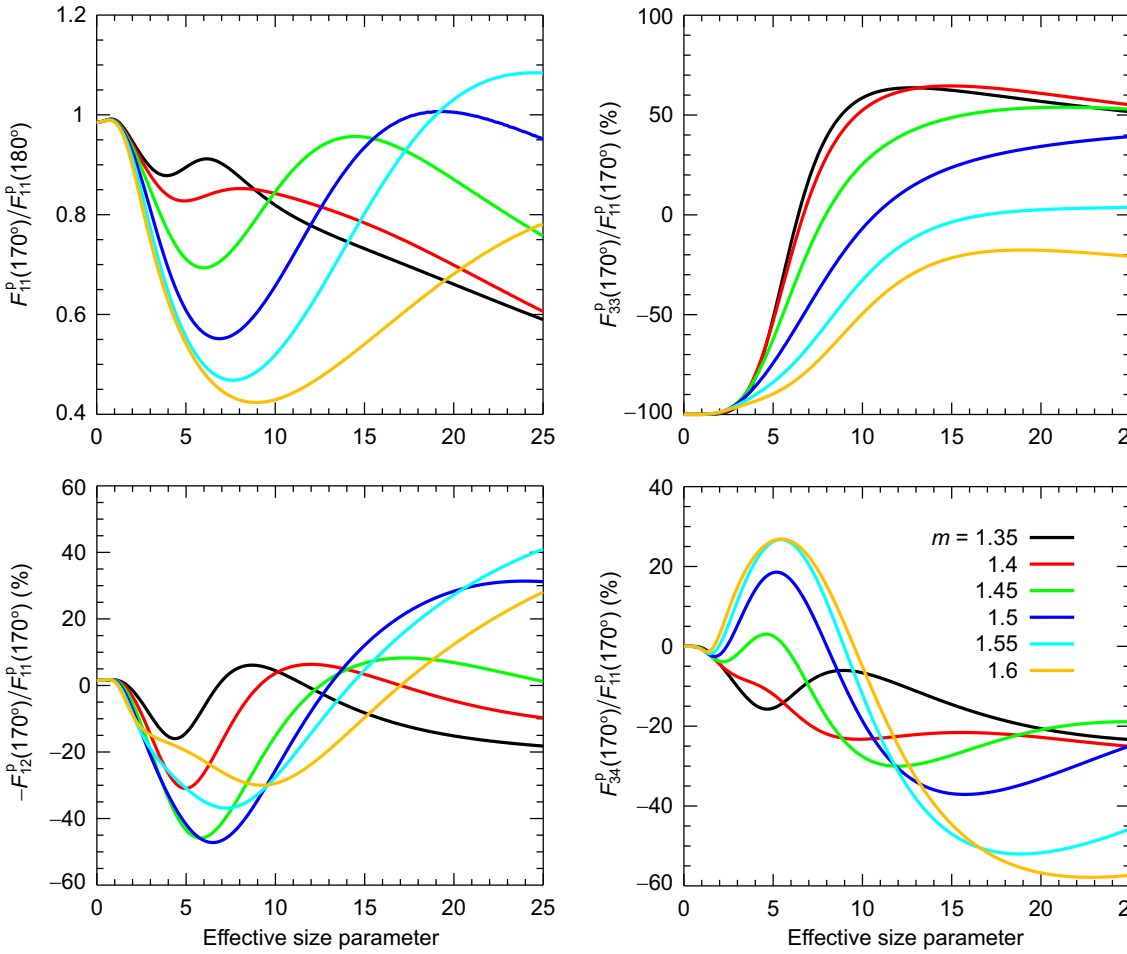

Fig. 6. Ratios of the elements of the particulate scattering matrix.

- Yield direct characterization of ground-level aerosols as atmospheric pollutants.
- Yield direct measurements of polarized bidirectional surface reflectance.

As part of future research, we plan to perform a comprehensive sensitivity study to examine representative multistatic lidar systems. We will expand the methodologies developed in [21,23] to quantify the information content of the measurements afforded by each system depending on the choice of spectral channels, polarizations, and viewing angle(s). Both elastic and HSRL receiver options will be explored and compared to determine whether an elastic lidar can be sufficient for the mission or the HSRL capability proves to be essential. This will help us identify optimal sets of measurements capable of reliably constraining the physical properties of atmospheric particles discussed in Section 1.

Special attention must be paid to the case of nonspherical aerosol and/or cloud particles. Even though the vast majority of nonspherical aerosols (e.g., dust grains and carbonaceous particles) are small enough to be randomly oriented, the equalities (11)–(13) and (18)–(20) no longer hold. As a consequence, the measurable quantities $F^V_{22}(180°)$, $F^V_{33}(180°)$, $F^V_{44}(180°)$, $F^p_{22}(180°)$, $F^p_{33}(180°)$, and $F^p_{44}(180°)$ can carry useful implicit information supplementary to that carried by $F^V_{11}(180°)$ and $F^p_{11}(180°)$ (see [34,45–47] and references therein). Of course, the complexity of modeling light-scattering properties of morphologically complex particles can often make this information difficult to extract.

Cirrus cloud particles belonging to a certain size/shape range can be made preferentially oriented in the horizontal plane by the aerodynamic force resulting from nonzero settling velocity. This can, in general, change the very structure of the cloud-particle scattering matrix. Another complication is that now the scattering medium is anisotropic so that the scalar transmission factor $T_2(\Theta)$ may have to be replaced by a 4×4 matrix propagator (see Section 10.2 of [17]), especially if the scattering angle substantially deviates from 180° [48–50]. This latter factor can speak in favor of selecting Θ values close to 180°. Of course, another advantage of a near-backscattering value of Θ is that it minimizes the effects of horizontal inhomogeneity in elastic lidar observations and makes Eq. (22) applicable in a wider range of atmospheric scenarios.

One could think of two technologically plausible types of a multi-satellite lidar system affording multistatic measurements. Both include a primary satellite equipped with a nadir-looking backscattering lidar. The first (bistatic) system also

includes a single secondary satellite with a state-of-the-art receiver having an optical-quality glass-mirror telescope. The secondary satellite may also host other instruments. The feasibility of a fully controlled two-satellite system has been successfully demonstrated by flying in formation the platforms carrying the Cloud–Aerosol Lidar with Orthogonal Polarization (CALIOP) [26] and the CloudSat radar [51] (see also [52]). Similar systems are being considered for the future National Aeronautics and Space Administration (NASA) Aerosol–Cloud–Ecosystem (ACE) space mission (http://acemission.gsfc.nasa.gov), which implies that the information content of aerosol and cloud measurements could be increased dramatically at the reasonable cost of putting another lidar receiver on the second platform.

In the second system, each of the $N \geq 1$ additional receivers is deployed on its own platform (with no additional payload). Technologically, this could be possible to achieve by combining relatively inexpensive identical CubeSats with light-weight inflatable mirrors. The technology for such mirrors was patented by NASA and was developed by the US Air Force (see, e.g., [53]), NASA's Jet Propulsion Laboratory ([54]), and L. Garde, Inc (http://www.lgarde.com).

There is no doubt that flying a multistatic (including bistatic) lidar system in space will pose certain engineering challenges. However, recent progress in building ground-based multistatic lidars [55–69] provides compelling reasons for optimism.

Finally we note that although the specific subject of this Perspective is the multistatic lidar concept, all our conclusions equally apply to a multistatic radar orbital system intended to study the global distribution of cloud and precipitation characteristics. In fact, one could think of a bistatic lidar–radar system wherein the backscattering lidar and the backscattering radar are carried by two formation-flying satellites with an extra receiver of the scattered laser light being placed on the radar satellite and an extra receiving antenna being placed on the lidar satellite.

Acknowledgments

We thank an anonymous reviewer for constructive suggestions, Igor Veselovskii for instructive discussions, and Nadia Zakharova for providing Figs. 2–6. This research was supported by the NASA ACE Project managed by Hal Maring and Arlindo da Silva.

References

[1] Ramaswamy V, Boucher O, Haigh J, Hauglustaine D, Haywood J, Myhre G, et al. Radiative forcing of climate change. In: Climate change 2001: the scientific basis. Cambridge, UK: Cambridge University Press; 2001. p. 349–416.
[2] Schulz M, Textor C, Kinne S, Balkanski Y, Bauer S, Berntsen T, et al. Radiative forcing by aerosols as derived from the AeroCom present-day and pre-industrial simulations. Atmos Chem Phys 2006;6:5225–46.
[3] Yu H, Kaufman YJ, Chin M, Feingold G, Remer LA, Anderson TL. A review of measurement-based assessments of the aerosol direct radiative effect and forcing. Atmos Chem Phys 2006;6:613–66.
[4] Hansen J, Sato M, Kharecha P, von Schuckmann K. Earth's energy imbalance and implications. Atmos Chem Phys 2011;11:13421–49.
[5] Chin M, Kahn RA, Schwartz SE, editors. Atmospheric aerosol properties and climate impacts. Washington, DC: US Climate Change Science Program; 2009.
[6] Li Z, Zhao X, Kahn R, Mishchenko M, Remer L, Lee K-H, et al. Uncertainties in satellite remote sensing of aerosols and impact on monitoring its long-term trend: a review and perspective. Ann Geophys 2009;27:2755–70.
[7] Loeb NG, Su W. Direct aerosol radiative forcing uncertainty based on a radiative perturbation analysis. J Clim 2010;23:5288–93.
[8] Lohmann U, Ferrachat S. Impact of parametric uncertainties on the present-day climate and on the anthropogenic aerosol effect. Atmos Chem Phys 2010;10:11373–83.
[9] Penner JE, Xu L, Wang M. Satellite methods underestimate indirect climate forcing by aerosols. Proc Natl Acad Sci USA 2011;108:13404–8.
[10] Chin M, Diehl T, Tan Q, Prospero JM, Kahn RA, Remer LA, et al. Multi-decadal aerosol variations from 1980 to 2009: a perspective from observations and a global model. Atmos Chem Phys 2014;14:3657–90.
[11] Schwartz SE. Uncertainty requirements in radiative forcing of climate change. J Air Waste Manag Assoc 2004;54:1351–9.
[12] Schwartz SE, Charlson RJ, Rhode H. Quantifying climate change—too rosy a picture? Nat Rep Clim Change 2007;1:23–4.
[13] Hansen J, Rossow W, Carlson B, Lacis A, Travis L, Del Genio A, et al. Low-cost long-term monitoring of global climate forcings and feedbacks. Clim Change 1995;31:247–71.
[14] Mishchenko MI, Cairns B, Kopp G, Schueler CF, Fafaul BA, Hansen JE, et al. Accurate monitoring of terrestrial aerosols and total solar irradiance: introducing the Glory Mission. Bull Am Meteorol Soc 2007;88:677–91.
[15] Mishchenko MI, Cairns B, Hansen JE, Travis LD, Burg R, Kaufman YJ, et al. Monitoring of aerosol forcing of climate from space: analysis of measurement requirements. J Quant Spectrosc Radiat Transf 2004;88:149–61.
[16] Hansen JE, Travis LD. Light scattering in planetary atmospheres. Space Sci Rev 1974;16:527–610.
[17] Mishchenko MI, Travis LD, Lacis AA. Multiple scattering of light by particles: radiative transfer and coherent backscattering. Cambridge, UK: Cambridge University Press; 2006. ⟨http://www.giss.nasa.gov/staff/mmishchenko/books.html⟩.
[18] Mishchenko MI, Travis LD. Satellite retrieval of aerosol properties over the ocean using measurements of reflected sunlight: effect of instrumental errors and aerosol absorption. J Geophys Res 1997;102:13543–53.
[19] Mishchenko M, Travis LD. Satellite retrieval of aerosol properties over the ocean using polarization as well as intensity of reflected sunlight. J Geophys Res. 1997;102:16989–7013.
[20] Mishchenko MI, Travis LD, Rossow WB, Cairns B, Carlson BE, Han Q. Retrieving CCN column density from single-channel measurements of reflected sunlight over the ocean: a sensitivity study. Geophys Res Lett 1997;24:2655–8.
[21] Knobelspiesse K, Cairns B, Mishchenko M, Chowdhary J, Tsigaridis K, van Diedenhoven B, et al. Analysis of fine-mode aerosol retrieval capabilities by different passive remote sensing instrument designs. Opt Express 2012;20:21457–84.
[22] McCormick MP. Airborne and spaceborne lidar. In: Weitkamp C, editor. Lidar: range-resolved optical remote sensing of the atmosphere. Berlin: Springer; 2005. p. 355–97.
[23] Chemyakin E, Burton S, Kolgotin A, Müller D, Hostetler C, Ferrare R. Retrieval of aerosol parameters from multiwavelength lidar: investigation of the underlying inverse mathematical problem. Appl Opt 2016;55:2188–202.
[24] Kovalev VA, Eichinger WE. Elastic lidar: theory, practice, and analysis methods. Hoboken, NJ: Wiley-Interscience; 2004.
[25] Weitkamp C, editor. Lidar: range-resolved optical remote sensing of the atmosphere. Berlin: Springer; 2005.
[26] Winker DM, Vaughan MA, Omar A, Hu Y, Powell KA, et al. Overview of the CALIPSO mission and CALIOP data processing algorithms. J Atmos Ocean Technol 2009;26:2310–23.
[27] Kovalev VA. Solutions in lidar profiling of the atmosphere. Hoboken, NJ: Wiley; 2015.
[28] Gross B, Moshary F, Arend M, editors. The 27th International Laser Radar Conference (ILRC 27). EPJ Web of Conferences, vol. 119, 2016. ⟨http://www.epj-conferences.org⟩.
[29] Whiteman DN, Perez-Ramirez D, Veselovskii I, Colarco P, Buchard V. Simulations of spaceborne multiwavelength lidar measurements

and retrievals of aerosol microphysics. Atmos Meas Tech Discuss 2016. http://dx.doi.org/10.5194/amt-2016-174.
[30] Rogers PJ, Eccles P. The bistatic radar equation for randomly distributed targets. Proc IEEE 1971;59:1019–21.
[31] Reagan JA, Byrne DM, Herman BM. Bistatic LIDAR: a tool for characterizing atmospheric particulates: Part I – The remote sensing problem. IEEE Trans Geosci Remote Sens 1982;20:229–35.
[32] Reagan JA, Byrne DM, Herman BM. Bistatic LIDAR: a tool for characterizing atmospheric particulates: Part II – The inverse problem. IEEE Trans Geosci Remote Sens 1982;20:236–43.
[33] van de Hulst HC. Light scattering by small particles. New York: Wiley; 1957.
[34] Mishchenko MI, Travis LD, Lacis AA. Scattering, absorption, and emission of light by small particles. Cambridge, UK: Cambridge University Press; 2002. 〈http://www.giss.nasa.gov/staff/mmishchenko/books.html〉.
[35] Hovenier JW, van der Mee C, Domke H. Transfer of polarized light in planetary atmospheres–basic concepts and practical methods. Dordrecht, The Netherlands: Kluwer; 2004.
[36] Mishchenko MI. Electromagnetic scattering by particles and particle groups: an introduction. Cambridge, UK: Cambridge University Press; 2014.
[37] Shipley ST, Tracy DH, Eloranta EW, Trauger JT, Sroga JT, Roesler FL, et al. A high spectral resolution lidar to measure optical scattering properties of atmospheric aersols. Part I: Intrumentation and theory. Appl Opt 1983;23:3716–24.
[38] Eloranta EE. High spectral resolution lidar. In: Weitkamp C, editor. Lidar: range-resolved optical remote sensing of the atmosphere. Berlin: Springer; 2005. p. 143–63.
[39] Hair JW, Hostetler CA, Cook AL, Harper DB, Ferrare RA, Mack TL, et al. Airborne High Spectral Resolution Lidar for profiling aerosol optical properties. Appl Opt 2008;47:6734–52.
[40] Veselovskii I, Kolgotin A, Griaznov V, Müller D, Wandinger U, Whiteman DN. Inversion with regularization for the retrieval of tropospheric aerosol parameters from multi-wavelength lidar sounding. Appl Opt 2002;41:3685–99.
[41] Su W, Schuster GL, Loeb NG, Rogers RR, Ferrare RA, Hostetler CA, et al. Aerosol and cloud interaction observed from high spectral resolution lidar data. J Geophys Res 2008;113:D24202.
[42] Veselovskii I, Dubovik O, Kolgotin A, Korenskiy M, Whiteman DN, Allakhverdie K, et al. Linear estimation of particle bulk parameters from multi-wavelength lidar measurements. Atmos Meas Tech 2012;5:1135–45.
[43] Müller D, Hostetler CA, Ferrare RA, Burton SP, Chemyakin E, Kolgotin A. Airborne Multiwavelength High Spectral Resolution Lidar (HSRL-2) observations during TCAP 2012: vertical profiles of optical and microphysical properties of a smoke/urban haze plume over the northeastern coast of the US. Atmos Meas Tech 2014;7:3487–96.
[44] Sawamura P, Moore RH, Burton SP, Chemyakin E, Müller D, et al. HSRL-2 aerosol optical measurements and microphysical retrievals vs. airborne in situ measurements during DISCOVER-AQ 2013: an intercomparison study. Atmos Chem Phys Discuss 2016. http://dx.doi.org/10.5194/acp-2016-380.
[45] Sassen K. Polarization in lidar. In: Weitkamp C, editor. Lidar: range-resolved optical remote sensing of the atmosphere. Berlin: Springer; 2005. p. 19–42.
[46] Burton SP, Hair JW, Kahnert M, Ferrare RA, Hostetler CA, Cook AL, et al. Observations of the spectral dependence of linear particle depolarization ratio of aerosols using NASA Langley airborne high spectral resolution lidar. Atmos Chem Phys 2015;15:13453–73.
[47] Dubovik O, Sinyuk A, Lapyonok L, Holben BN, Mishchenko M, Yang P, et al. Application of spheroid models to account for aerosol particle nonsphericity in remote sensing of desert dust. J Geophys Res 2006;111:D11208.
[48] Shefer O. Numerical study of extinction of visible and infrared radiation transformed by preferentially oriented plate crystals. J Quant Spectrosc Radiat Transf 2013;117:104–13.
[49] Gao M, Yang P, Kattawar GW. Polarized extinction properties of plates with large aspect ratios. J Quant Spectrosc Radiat Transf 2013;131:72–81.
[50] Shefer O. Extinction of radiant energy by large atmospheric crystals with different shapes. J Quant Spectrosc Radiat Transf 2016;178:350–60.
[51] Stephens GL, Vane DG, Boain RJ, Mace GG, Sassen K, Wang Z, et al. The CloudSat Mission and the A-Train: a new dimension of space-based observations of clouds and precipitation. Bull Am Meteorol Soc 2002;83:1771–90.
[52] Krieger G, Moreira A, Fiedler H, Hajnsek I, Werner M, Younis M, et al. TanDEM-X: a satellite formation for high-resolution SAR interferometry. IEEE Trans Geosci Remote Sens 2007;45:3317–41.
[53] Wagner JW. Optical metrology of adaptive membrane mirrors-Wright–Patterson Air Force Base, OH: Air Force Institute of Technology; 2000.
[54] Meinel AB, Meinel MP. Inflatable membrane mirrors for optical passband imagery. Opt Eng 2000;39:541–50.
[55] Parameswaran K, Rose KO, Krishna Murthy BV. Aerosol characteristics from bistatic lidar observations. J Geophys Res 1984;89:2541–52.
[56] Devara PCS, Ernest Raj P. Remote sounding of aerosols in the lower atmosphere using a bistatic CW helium–neon lidar. J Aerosol Sci 1989;20:37–44.
[57] Welsh BM, Gardner CS. Bistatic imaging lidar technique for upper atmospheric studies. Appl Opt 1989;28:82–8.
[58] Meki K, Yamaguchi K, Li X, Saito Y, Kawahara TD, Nomura A. Range-resolved bistatic imaging lidar for the measurement of the lower atmosphere. Opt Lett 1996;21:1318–20.
[59] Sugimoto N. Two-color dual-polarization pulsed bistatlc lidar for measuring water cloud droplet size. Opt Rev 2000;7:235–40.
[60] Sugimoto N, Matsui I, Shimizu A. Measurement of water cloud particle size with a dual-polarization pulsed bistatic lidar. Opt Rev 2001;8:476–9.
[61] Barnes JE, Bronner S, Beck R, Parikh NC. Boundary layer scattering measurements with a charge-coupled device camera lidar. Appl Opt 2003;42:2647–52.
[62] Novitsky EJ, Philbrick CR. Multistatic lidar profiling of urban atmospheric aerosols. J Geophys Res 2005;110:D07S11.
[63] Barnes JE, Parikh Sharma NC, Kaplan TB. Atmospheric aerosol profiling with a bistatic imaging lidar system. Appl Opt 2007;46:2922–9.
[64] Olofson KFG, Witt G, Pettersson JBC. Bistatic lidar measurements of clouds in the Nordic Arctic region. Appl Opt 2008;47:4777–86.
[65] Olofson KFG, Svensson EA, Witt G, Pettersson JBC. Arctic aerosol and clouds studied by bistatic lidar technique. J Geophys Res 2009;114:D18208.
[66] Wyant AM, Brown DM, Edwards PS, Philbrick CR. Multi-wavelength multi-angular lidar for aerosol characterization. Proc SPIE 2009;7323:73230R.
[67] Sharma NCP, Barnes JE, Kaplan TB, Clarke AD. Coastal aerosol profiling with a camera lidar and nephelometer. J Atmos Ocean Technol 2011;28:418–25.
[68] Lv L, Zhang T, Liu C, Dong Y, Chen Z, Fan G, et al. Atmospheric aerosols detection research with a dual field of view lidar. J Spectrosc 2015;2015:459460.
[69] Wang Z, Tao Z, Liu D, Wu D, Xie C, Wang Y. New experimental method for lidar overlap factor using a CCD side-scatter technique. Opt Lett 2015;40:1749–52.